ARCHIVES OF MECHANICS
Arch. Mech. **78** (∗), ∗∗∗–∗∗∗, 2026, https://doi.org/10.24423/aom.4895

Instability of the Navier–Stokes–Voigt fluid flow with couple stresses effect

S. S. HAJOOL, A. J. HARFASH

Department of Mathematics, College of Sciences, University of Basrah, Basrah, Iraq, e-mails: shahizlan.shakir@gmail.comm, akilharfash@gmail.com

This study examines the linear instability in a channel flow of the Navier–Stokes–Voigt viscoelastic fluid, influenced by couple stresses. It confirms the applicability of Squire's theorem and develops a generalized eigenvalue problem for two-dimensional modes using two Chebyshev collocation methods. This problem is then solved with the QZ algorithm. Despite the base flow maintaining characteristics of the Newtonian fluid, the instability of the fluid flow is significantly affected by the presence of the Kelvin–Voigt parameter and the couple stresses parameter. Numerical results showed the effect of increasing the couple stresses and the Kelvin–Voigt parameters on the stability of the system. As the value of these parameters increases, the critical values of the Reynolds number begin to increase, which initially indicates a stabilising effect.

Key words: Poiseuille flow, couple stresses, Navier–Stokes–Voigt, linear instability, Chebyshev collocation.

1. Introduction

The investigation of the stability and instability of classical laminar flows of incompressible fluids has garnered significant interest from researchers, both theoretically and experimentally, due to its relevance in various physical contexts, including astrophysics, meteorology, oceanography, geophysics, and engineering [1]. Understanding the transitions of laminar flow into unstable and chaotic flow is far from complete, leading to its ongoing importance as a research topic. Inspired by Reynolds' work, in [2, 3], it has independently conducted theoretical studies, leading to the derivation of the Orr–Sommerfeld equation by analyzing small, traveling-wave perturbations in a steady, parallel flow. This equation, when applied to plane Poiseuille flow, indicates instability. Research on the stability of plane Poiseuille flow has expanded in various directions, considering factors such as the effects of a transverse magnetic field [4, 5], throughflow [6], and its counterpart in porous media [7–16]. In addition to the above references, there are many other studies that included the study of fluid flow problems [17–21].

Couple stresses are instrumental in dissecting the mechanical behaviour and flow dynamics of complex fluids that contain microstructures, such as suspensions, polymeric solutions, and non-Newtonian fluids. Couple stress fluids provide a more elaborate account of fluid flow behavior, by considering the inherent rotation of molecules in their microstructure, which is not included in the classical definition of the vorticity field. The micropolar fluid model includes a vectorial microrotation field along with an extra set of three constitutive relations, whereas the model for couple stress fluid assumes the proportionality of the microrotation to the vorticity. In this way, the three-dimensional quantity is reduced to one scalar quantity. In fluids with microscopic characteristics, couple stresses offer additional stress factors compared to ordinary shear stresses. This influences how the fluid reacts to external stimuli and, in some instances, might even cause the fluid's constituent parts to align. This orientation might change the fluid's effective viscosity, and thus it would have an impact on laminar stability, turbulence transition, as well as velocity profiles in pipes and channel flow [22].

Couple stresses explain tiny rotations inside fluids that affect heat, mechanical force, energy dissipation, and even more than just fluid motion. They can also change the way boundary layers are formed just before solid surfaces [23]. Due to the significant effects of couple stresses, typical fluid mechanics models may fail in complicated geometries or porous materials [24]. First of all, they are very important in the scattering and orientation of particles in suspensions, which determines how these mixtures flow and settle [25]. Couple stresses represent a fascinating topic of research which is opening new perspectives in the field of fluid dynamics. Several convection models have been studied lately to demonstrate how these stresses affect stability and instability conditions [26–28].

Traditional fluid dynamics models, which rely on the Navier–Stokes equations, find it very challenging to depict complex fluid behaviour. In contrast to simple fluids, such fluids exhibit a "memory" effect. In fact, their response to stress depends not only on the current turnover of velocity but also on the past one. Hence, researchers have been motivated to formulate novel theories that would lead to a more accurate description of viscoelastic fluids. A couple of very recent research papers [29, 30] have delved into the complex behaviour of these fluids and thus provide very useful information about their unique features.

The majority of current research has focused on complex viscoelastic materials, particularly those categorized as Voigt–Kelvin materials. Publications such as [31] highlight important improvements to the subject that have significantly influenced our comprehension of these items. Theory for Kelvin–Voigt fluids have been developed, firstly in the studies of [32], and have been significant in improving our understanding of the dynamic behaviour of these viscoelastic materials. These fluids are fascinating because they can replicate the behaviour

of materials in everyday life. In contrast to more basic mathematical models, stress relies on both the present condition and the deformation history of the material. In particular, this study explores Kelvin–Voigt systems with thermal effects, as thoroughly discussed in [33]. It is essential to comprehend how heat affects the mechanical characteristics of viscoelastic materials, and [33] offers a useful starting point for this investigation. This research focuses on the Navier–Stokes–Voigt equations, which take couple stress effect into account. Recent research has studied stability and instability for some convection models under the effect of couple stresses [34–40]. These studies provide detailed understandings of the behaviour of Kelvin–Voigt medium that in turn help in the control and development of complex systems for real, world applications.

Although instabilities related to Kelvin–Voigt fluids of different orders have been extensively studied in horizontal Bénard type geometries (free convection), the hydrodynamic stability (forced convection) of such fluid flows has not yet received significant attention in the literature. Researchers focus heavily on the transition from laminar to turbulent regimes in viscoelastic flows due to their application in various technological processes and the potential for significant reductions in turbulent friction in dilute polymer solutions. Understanding the combined effects of inertia and viscoelasticity is crucial for the phenomenon of turbulent drag reduction in parallel shear flows [41]. This study aims to analyze the stability of plane Poiseuille flow of the Kelvin–Voigt fluid of order zero, also known as the Navier–Stokes–Voigt fluid. The neutral stability condition and the critical Reynolds number are determined for various values of viscoelasticity controlling parameters, revealing some novel results not found in other types of viscoelastic fluid flows. There are wider uses for the insights gained from researching the instability of Navier–Stokes–Voigt fluids with couple stresses. Fluid mechanics is not the only discipline it affects; it also has an impact on materials science, which helps us figure out how materials flow, biomedical engineering, which helps us build better biomaterials, and environmental science, which helps us create models that mimic the movement of pollutants in water.

In [42], it has analyzed the temporal stability features of plane Poiseuille and plane Couette configurations for a viscoelastic fluid that obeys the Navier–Stokes–Voigt model. Basically, the set up is a flow between two infinitely long, rigid and parallel plates that can be either fixed or moving relative to one another. Besides that, [43] investigates linear stability of a pressure, driven channel flow of an electrically conducting viscoelastic fluid that is modeled by the same Navier–Stokes–Voigt system, and the influence of a transverse magnetic field which is externally applied, is also considered.

The work essentially delves into the linear stability analysis of a pressure, induced channel flow of a Navier–Stokes–Voigt type viscoelastic fluid in the presence of couple stresses. The mathematical formulation of the problem leads

to a generalized eigenvalue problem for two, dimensional perturbations which is solved numerically through the QZ algorithm. While the base flow of the fluid shows characteristics similar to those of a Newtonian fluid, the stability traits get largely affected by the Kelvin–Voigt parameter and the couple stresses parameter, as well. The obtained results reveal, that, physically unstable modes can develop only in a restricted range of the Kelvin–Voigt parameter and, moreover, the degree of instability is strongly influenced by the value of the couple stresses parameter.

In the next section, we present the mathematical model of the problem under study, followed by presenting the steady solution to the problem, for which instability is studied. Also, perturbation variables and equations governing for perturbations are presented. This is followed by the derivation of linear instability equations in Section 3. Section 4 is concerned with presenting the proposed numerical methods for solving the system of eigenvalues resulting from linear instability analysis, where two methods are proposed and the advantages and disadvantages of using both methods are discussed in detail. Section 5 presented the numerical results that were calculated and analyzed these results in detail. The last section was dedicated to mentioning the conclusions we reached through this study.

2. Mathematical model

In this study, we investigate the couple stress effects in a pressure driven Poiseuille-type flow. The flow fills the area $(x, y) \in \mathbb{R}^2$ and $z \in (-H, H)$, and the motion is for $t > 0$. The fluid motion in this region is determined by the following equations of motion:

$$\begin{gathered} \rho((1-\hat{\lambda}\Delta)\widetilde{\mathbf{v}}_{,t} + (\widetilde{\mathbf{v}}\cdot\nabla)\widetilde{\mathbf{v}}) = -\nabla\widetilde{\mathrm{p}} + \mu\Delta\widetilde{\mathbf{v}} - \hat{\mu}\Delta^2\widetilde{\mathbf{v}}, \\ \nabla\cdot\widetilde{\mathbf{v}} = 0. \end{gathered} \tag{2.1}$$

Here, the quantities $\widetilde{\mathbf{v}}$, $\widetilde{\mathrm{p}}|$, ρ, $\hat{\lambda}$, μ, and $\hat{\mu}$ are the velocity vector, pressure, fluid density, Kelvin–Voigt parameter, effective (dynamic) viscosity, and the viscosity related to couple stresses, respectively; refer to [7, 44, 45] for more details. The system is also supplemented by the following boundary conditions:

$$\widetilde{\mathbf{v}} = 0 \quad \text{on } z = \pm H. \tag{2.2}$$

Introducing characteristic scales H for the length, $\widetilde{V}_0$ for the velocity magnitude, $H/\widetilde{V}_0$ for time and $\mu\widetilde{V}_0/H$ for pressure, the governing equations (2.1) are made dimensionless as follows:

$$\begin{gathered} \mathrm{Re}[(1-\eta\Delta)\widetilde{\mathbf{v}}_{,t} + (\widetilde{\mathbf{v}}\cdot\nabla)\widetilde{\mathbf{v}}] = -\nabla\widetilde{\mathrm{p}} + \Delta\widetilde{\mathbf{v}} - K\Delta^2\widetilde{\mathbf{v}}, \\ \nabla\cdot\widetilde{\mathbf{v}} = 0. \end{gathered} \tag{2.3}$$

Here, Re denotes the Reynolds number, which measures the ratio of inertial forces to viscous forces within the fluid, η is the dimensionless Kelvin–Voigt parameter, K represents a dimensionless coefficient of couple stress viscosity, which are defined by the following relationships:

$$Re = \frac{\rho H \widetilde{V}_0}{\mu}, \quad \eta = \frac{\hat{\lambda}}{H^2}, \quad K = \frac{\hat{\mu}}{\mu H^2}.$$

The equations apply within the domain $(x, y) \in \mathbb{R}^2 \times z \in (-1, 1) \times t > 0$. The associated boundary conditions are as follows:

$$\widetilde{\mathbf{v}} = 0 \quad \text{on } z = \pm 1. \tag{2.4}$$

The fluid movement occurs in the space between two infinitely long horizontal plates which are positioned parallel to each other at $z = -1$ and $z = 1$. Both plates are fixed and do not move. The flow of the fluid is propelled by a uniform pressure gradient E directed along the positive x-axis. This force is described mathematically by the following expression:

$$-\frac{\partial \overline{\mathrm{p}}}{\partial x} = E > 0.$$

In the context of this formulation, variables decorated with an overbar indicate their steady, state values. The base flow is considered to be fully developed, steady, laminar, and unidirectional along the spatial axis. Hence, it is written as $\overline{\mathbf{v}}_B = (\overline{U}_B(z), 0, 0)$ with the subscript (B) denoting the base (or basic) state. Making these assumptions, Eq. (2.4) reduces to the following ordinary differential equation:

$$(\overline{U}_B)''(z) - K(\overline{U}_B)^{(4)}(z) + E = 0, \tag{2.5}$$

with no-slip boundary conditions:

$$(\overline{U}_B)''(z) = 0, \quad \overline{U}_B(z) = 0, \quad z = \pm 1. \tag{2.6}$$

By solving Eq. (2.5) and applying the boundary conditions (2.6), we derive the following solutions:

$$\overline{U}_B(z) = E\left[\frac{K\cosh\left(\frac{z}{\sqrt{K}}\right)}{\cosh\left(\frac{1}{\sqrt{K}}\right)} - K + \frac{1}{2}(1 - z^2)\right]. \tag{2.7}$$

In the equation mentioned, E represents the pressure gradient, which is determined from the centerline velocity as detailed in [7]. The calculation of E is outlined as follows:

$$E = \frac{2\cosh\left(\frac{1}{\sqrt{K}}\right)}{2K\left[1 - \cosh\left(\frac{1}{\sqrt{K}}\right)\right] + \cosh\left(\frac{1}{\sqrt{K}}\right)}. \tag{2.8}$$

Substituting (2.8) into (2.7) produces the following result:

$$\overline{U}_B(z) = \frac{2K\big[\cosh\big(\frac{z}{\sqrt{K}}\big) - \cosh\big(\frac{1}{\sqrt{K}}\big)\big] + \cosh\big(\frac{1}{\sqrt{K}}\big)[1-z^2]}{2K\big[1-\cosh\big(\frac{1}{\sqrt{K}}\big)\big] + \cosh\big(\frac{1}{\sqrt{K}}\big)}. \tag{2.9}$$

In the limiting case $K \to 0$, the model reduces to the classical scenario, and the associated no-slip base profile becomes $\overline{U}_B(z) = 1 - z^2$, which coincides with the well-known parabolic Poiseuille solution reported in [1].

We consider perturbations $\mathbf{u} = (u, v, w)$ and Π with respect to the steady solutions $\overline{U}_B$ and $\overline{\mathrm{p}}_B$, respectively. These perturbations are expressed in the following form:

$$v_1 = \overline{U}_B + u, \quad \widetilde{v}_2 = v, \quad \widetilde{v}_3 = w, \quad \widetilde{\mathrm{p}} = \overline{\mathrm{p}}_B + \Pi. \tag{2.10}$$

Inserting (2.10) into (2.3) yields the following equations for the disturbances:

$$\begin{aligned} \mathrm{Re}[(1-\eta\Delta)\mathbf{u}_{,t} + (\mathbf{u}\cdot\nabla)\mathbf{u} + (\overline{U}_B\cdot\nabla)\mathbf{u} + (\mathbf{u}\cdot\nabla)\overline{U}_B] \\ = -\nabla\Pi + \triangle\mathbf{u} - K\Delta^2\mathbf{u}, \\ \nabla\cdot\mathbf{u} = 0. \end{aligned} \tag{2.11}$$

3. Stability analysis

We ignore the nonlinear terms in Eq. (2.11) to explore linear instability, which gives us the following linear system:

$$\begin{aligned} \mathrm{Re}[(1-\eta\Delta)\mathbf{u}_{,t} + (\overline{U}_B\cdot\nabla)\mathbf{u} + (\mathbf{u}\cdot\nabla)\overline{U}_B] = -\nabla\Pi + \triangle\mathbf{u} - K\Delta^2\mathbf{u}, \\ \nabla\cdot\mathbf{u} = 0. \end{aligned} \tag{3.1}$$

As $\mathbf{u} = (u, v, w)$, the representation of (3.1) can be as follows:

$$\begin{aligned} \mathrm{Re}\big[(1-\eta\Delta)u_{,t} + \overline{U}_B u_{,x} + w(\overline{U}_B)'\big] &= -\Pi_{,x} + \Delta u - K\Delta^2 u, \\ \mathrm{Re}\big[(1-\eta\Delta)v_{,t} + \overline{U}_B v_{,x}\big] &= -\Pi_{,y} + \Delta v - K\Delta^2 v, \\ \mathrm{Re}\big[(1-\eta\Delta)w_{,t} + \overline{U}_B w_{,x}\big] &= -\Pi_{,z} + \Delta w - K\Delta^2 w, \\ u_{,x} + v_{,y} + w_{,z} &= 0. \end{aligned} \tag{3.2}$$

The conditions for the boundaries are

$$u = v = w = 0 \quad \text{on } z = \pm 1. \tag{3.3}$$

To analyze linear instability using the equations in (3.2), the normal modes approach is utilized. This method assumes that the perturbation velocity and pressure fields are of the form $\exp[i\beta y + i\alpha(x - ct)]$, representing a wave-like dis-

turbance propagating through the medium. In a similar way, the stream function of the disturbance velocity that contains the velocity components u, v, and w, is given by:

$$\{u, v, w, \Pi\}(x, y, z, t) = \{u, v, w, \Pi\}(z) \exp[i\beta y + i\alpha(x - ct)]. \tag{3.4}$$

In Eq. (3.4), $\{u, v, w, \Pi\}(z)$ refer to the amplitude components of the stream function, while α and β are the horizontal and vertical wave numbers, respectively. The complex parameter c accounts for both the wave speed (its real part) and the growth rate of the disturbance (its imaginary part). The moment when the growth rate is zero determines the point of transition from stability to instability of the flow, and such a condition is called neutral stability. Thus, substituting Eq. (3.4) into Eqs. (3.2) results in the following:

$$\begin{aligned} \mathrm{Re}\big\{ & i\alpha\big(\overline{U}_B - [1 - \eta(D^2 - \alpha^2 - \beta^2)]c\big)u + w(\overline{U}_B)'\big\} \\ & = -i\alpha\Pi + (D^2 - \alpha^2 - \beta^2)u - K(D^2 - \alpha^2 - \beta^2)^2 u, \end{aligned} \tag{3.5}$$

$$\begin{aligned} \mathrm{Re}\big\{ & i\alpha\big(\overline{U}_B - [1 - \eta(D^2 - \alpha^2 - \beta^2)]c\big)v\big\} \\ & = -i\beta\Pi + (D^2 - \alpha^2 - \beta^2)v - K(D^2 - \alpha^2 - \beta^2)^2 v, \end{aligned} \tag{3.6}$$

$$\begin{aligned} \mathrm{Re}\big\{ & i\alpha\big(\overline{U}_B - [1 - \eta(D^2 - \alpha^2 - \beta^2)]c\big)w\big\} \\ & = -D\Pi + (D^2 - \alpha^2 - \beta^2)w - K(D^2 - \alpha^2 - \beta^2)^2 w, \end{aligned} \tag{3.7}$$

$$i(\alpha u + \beta v) + Dw = 0, \tag{3.8}$$

where $D = d/dz$ is the differential operator. The corresponding boundary conditions are

$$u = v = w = 0 \quad \text{on } z = \pm 1. \tag{3.9}$$

Takashima's work in [46, 47] highlights that the three-dimensional problem described can be simplified to a two-dimensional one using a modified version of Squire's theorem. Specifically, this involves setting $a^2 = \alpha^2 + \beta^2$, $a\hat{u} = \alpha u + \beta v$, $a\,\hat{\mathrm{Re}} = \alpha\,\mathrm{Re}$, $a\hat{w} = \alpha w$ and $\hat{\Pi} = \Pi$, in Eqs. (3.5) through (3.9), after adding [(3.5) $\times\, \alpha$ with (3.6) $\times\, \beta$]. Consequently, Eqs. (3.5) through (3.9) are simplified to:

$$\begin{aligned} & ia^2\hat{\mathrm{Re}}\big(\overline{U}_B - [1 - \eta(D^2 - a^2)]c\big)\hat{u} + a\hat{w}\hat{\mathrm{Re}}(\overline{U}_B)' \\ & \qquad = -ia^2\hat{\Pi} + (D^2 - a^2)a\hat{u} - K(D^2 - a^2)^2 a\hat{u}, \end{aligned} \tag{3.10}$$

$$\begin{aligned} & ia\hat{\mathrm{Re}}\big(\overline{U}_B - [1 - \eta(D^2 - a^2)]c\big)\hat{w}\big\} \\ & \qquad = -D\hat{\Pi} + (D^2 - a^2)\hat{w} - K(D^2 - a^2)^2 \hat{w}, \end{aligned} \tag{3.11}$$

$$ia\hat{u} + D\hat{w} = 0. \tag{3.12}$$

By applying the continuity equations (3.12), one can eliminate Π, there by deriving a pair of equations that only involve w. This reduction is achieved by subtracting Eq. (3.11) multiplied by ia^2 from the z-derivative of Eq. (3.10). The equations that result from this process are:

$$\big(\overline{U}_B - c[1-\eta(D^2-a^2)]\big)(D^2-a^2)w - w(\overline{U}_B)'' = \frac{1}{iaRe}(D^2-a^2)^2 w - \frac{K}{iaRe}(D^2-a^2)^3 w. \tag{3.13}$$

Furthermore, the boundary conditions include the following expression:

$$w = Dw = D^3 w = 0 \quad \text{on } z = \pm 1. \tag{3.14}$$

4. Numerical method

The stability eigenvalue problem described by Eqs. (3.13) and (3.14), resulting from the form of the boundary conditions and the presence of the functions $\overline{U}_B$ and $(\overline{U}_B)''$ in the system, requires numerical solutions, as analytical methods are not feasible. Various numerical methods have been used to solve eigenvalue problems such as this one, and a lot of research work has been devoted to summarizing such methods in [1]. One of those methods is the shooting method, which is simple to understand but has real practical problems, for example, the need for a very accurate guess for the initial eigenvalue and the fact that only one eigenvalue can be followed at a time. The compound matrix method is another alternative that can be found in [48–50], and it is normally considered a better method than the shooting methods [49]. Nevertheless, it will not give you a general picture of the entire eigenvalue spectrum. The finite difference method is easy to understand and can be used in many situations but, it is often the case that people do not use it because it requires a very fine spatial and temporal discretization that can lead to extremely high computational costs as well as considerable demands on computer memory. One of the techniques that is continuously referred to, is the Chebyshev collocation method [51] which is one of the best methods among others in this field according to the literature. This is a very powerful method as it provides exponential convergence with very few collocation points and thus mitigates most of the difficulties encountered with other methods. Recently, there have been several papers reporting the use of this method to tackle the eigenvalue systems of hydrodynamic stability problems [52–57].

With the introduction of the functions $\Omega = Dw$ and $\Lambda = D^3 w$, the system in (3.13) can be reformulated as follows:

$$
\begin{aligned}
Dw - \Omega &= 0,\\
D^2\Omega - \Lambda &= 0,\\
\big[a^4 + Ka^6 + ia^3\,\mathrm{Re}(\overline{U}_B) + ia\,\mathrm{Re}(\overline{U}_B)''\big]w&\\
-\big[2a^2 + 3a^4K + ia\,\mathrm{Re}(\overline{U}_B)\big]D\Omega + \big[D + 3a^2KD - KD^3\big]\Lambda&\\
= -ia\,\mathrm{Re}\,c\big[(D\Omega - a^2w) - \eta(D\Lambda - 2a^2D\Omega + a^4w)\big].&
\end{aligned}
\tag{4.1}
$$

Based on the revised definitions, the boundary conditions (3.12) are reformulated as follows:

$$
w = \Omega = \Lambda = 0, \qquad z = \pm 1. \tag{4.2}
$$

In the following analysis, we introduce two methods to numerically verify the results of the eigenvalue system. Both methods are capable of approximating the solution with high precision. The key difference between them lies in their approaches to integrating boundary conditions and in their strategies for improving accuracy by increasing the number of polynomials used.

4.1. Method I

In this method, we represent the solutions to Eqs. (4.1) and (4.2) using a finite series of Chebyshev polynomials. Therefore, the solutions can be described as follows:

$$
w(z) = \sum_{\xi=0}^{\Xi+2} w_\xi T_\xi(z), \qquad \Omega(z) = \sum_{\xi=0}^{\Xi+2} \Omega_\xi T_\xi(z), \qquad \Lambda(z) = \sum_{\xi=0}^{\Xi+2} \Lambda_\xi T_\xi(z), \tag{4.3}
$$

where $T_\xi(z)$ denotes the Chebyshev polynomial of the first kind, defined as follows:

$$
T_\xi(z) = \cos(\xi \arccos(z)), \qquad -1 \le z \le 1.
$$

Subsequently, by substituting (4.3) into (4.1) and (4.2), and verifying that the resulting equations adhere to the Gauss–Lobatto points, which are characterized as

$$
y_\xi = \cos\left(\frac{\xi\pi}{\Xi}\right), \qquad \xi = 0, \ldots, \Xi. \tag{4.4}
$$

Here, Ξ represents the number of Chebyshev polynomials used in the spectral expansion in total, with Ξ being a positive integer. The indices $\xi = 0$ and $\xi = \Xi$ refer to the lower and upper wall boundaries, respectively. As a result of the discretization process, it is possible to derive $3\Xi, 3$ algebraic relations that involve $3\Xi + 3$ unknown coefficients, i.e., $w_0, \ldots, w_{\Xi+2}$, $\Omega_0, \ldots, \Omega_{\Xi+2}$, and

$\Lambda_0, \ldots, \Lambda_{\Xi+2}$. The system is closed by adding six more equations through the implementation of the specified boundary conditions, which are:

$$S_1: \sum_{\xi=0}^{\Xi+2} w_\xi = 0, \quad S_2: \sum_{\xi=0}^{\Xi+2} (-1)^\xi w_\xi = 0,$$
$$S_3: \sum_{\xi=0}^{\Xi+2} \Omega_\xi = 0, \quad S_4: \sum_{\xi=0}^{\Xi+2} (-1)^\xi \Omega_\xi = 0,$$
$$S_5: \sum_{\xi=0}^{\Xi+2} \Lambda_\xi = 0, \quad S_6: \sum_{\xi=0}^{\Xi+2} (-1)^\xi \Lambda_\xi = 0.$$

The discretized forms of the boundary conditions are combined directly with the algebraic eigenvalue framework, thus resulting in a square system of size $(3\Xi + 3) \times (3\Xi + 3)$. Through this formulation, the entire eigenvalue problem can be illustrated in matrix form and is given by:

$$\begin{pmatrix} \mathbb{D} & -I & M_0 \\ S_1 & V_0 & V_0 \\ S_2 & V_0 & V_0 \\ M_0 & \mathbb{D}^2 & -I \\ V_0 & S_3 & V_0 \\ V_0 & S_4 & V_0 \\ \varpi_{11} & \varpi_{12} & \varpi_{13} \\ V_0 & V_0 & S_5 \\ V_0 & V_0 & S_6 \end{pmatrix} X \tag{4.5}$$
$$= c \begin{pmatrix} M_0 & M_0 & M_0 \\ V_0 & V_0 & V_0 \\ V_0 & V_0 & V_0 \\ M_0 & M_0 & M_0 \\ V_0 & V_0 & V_0 \\ V_0 & V_0 & V_0 \\ ia^3 \operatorname{Re} + ia^5 \operatorname{Re} \eta & -(ia \operatorname{Re} + 2ia^3 \operatorname{Re} \eta)\mathbb{D} & ia \operatorname{Re} \eta \mathbb{D} \\ V_0 & V_0 & V_0 \\ V_0 & V_0 & V_0 \end{pmatrix} X,$$

where M_0 and V_0 are the zeros matrix and vector, respectively,

$$X = (w_0, \ldots, w_{\Xi+2}, \Omega_0, \ldots, \Omega_{\Xi+2}, \Lambda_0, \ldots, \Lambda_{\Xi+2}),$$
$$\varpi_{11}(\xi_1, \xi_2) = [a^4 + a^6 K + ia \operatorname{Re}(\overline{U}_B(y_{\xi_1})a^2 + (\overline{U}_B)''(y_{\xi_1}))]I(\xi_1, \xi_2),$$
$$\varpi_{12}(\xi_1, \xi_2) = -[2a^2 + 3a^4 K + ia \operatorname{Re} \overline{U}_B(y_{\xi_1})]\mathbb{D}(\xi_1, \xi_2),$$
$$\varpi_{13}(\xi_1, \xi_2) = [1 + 3a^2 K]\mathbb{D}(\xi_1, \xi_2) - K\mathbb{D}^3(\xi_1, \xi_2),$$

$$I(\xi_1,\xi_2)=T_{\xi_2}(y_{\xi_1}),$$
$$\mathbb{D}(\xi_1,\xi_2)=T'_{\xi_2}(y_{\xi_1}),\quad \mathbb{D}^2(\xi_1,\xi_2)=T''_{\xi_2}(y_{\xi_1}),$$
$$\mathbb{D}^3(\xi_1,\xi_2)=T'''_{\xi_2}(y_{\xi_1}),\quad \xi_1=0,\dots,\Xi,\quad \xi_2=0,\dots,\Xi+2.$$

The MATLAB software was used to calculate the matrix values, followed by the determination of the eigenvalues and the performance of all additional calculations.

4.2. Method II

Method II shows a major step forward over Method I in that it changes the depiction of solutions to be a linear combination of only a limited number of functions. These functions, obtained from Chebyshev polynomials, satisfy the boundary conditions automatically, thus there is no need to explicitly impose them in Method I as there was. In an effort to raise the level of accuracy while using fewer polynomials, Method II is different from Method I in that Method I increments by 1 only, whereas Method II utilizes both odd and even Chebyshev polynomials, doubling their order by 2. Thus, system solutions are composed as follows:

$$w=\sum_{\xi=0}^{\Xi} w_\xi\theta_\xi(z),\quad \Omega=\sum_{\xi=0}^{\Xi}\Omega_\xi\phi_\xi(z),\quad \Lambda=\sum_{\xi=0}^{\Xi}\Lambda_\xi\phi_\xi(z), \tag{4.6}$$

where θ_ξ and ϕ_ξ are defined by

$$\theta_\xi(z)=(1-z^2)T_{2\xi-2}(z),\quad \phi_\xi(z)=(1-z^2)T_{2\xi-1}(z). \tag{4.7}$$

In Method II the operator $T_\xi(z)$ defined in Method I is taken as a basis with θ_ξ and ϕ_ξ being the basis functions. The choice ensures that the solutions for w, Ω and Λ automatically satisfy the boundary conditions of Eq. (4.2). This clever move not only makes the process easier but also embeds the solvent to be consistent with boundary conditions right from the solvent framework thus no further changes or revisions are necessary.

After this, Eq. (4.6) is integrated into (4.1). Following this integration, the Gauss–Lobatto points are utilised, which are defined as follows:

$$y_\xi=\cos\big[(\xi-1)/(2\Xi-1)\pi\big],\quad \xi=0,\dots,\Xi. \tag{4.8}$$

Using the Gauss–Lobatto collocation points and substituting θ_ξ and ϕ_ξ in the governing equations, the continuous problem is transformed into a finite number of algebraic equations. The system obtained is of size $3(\Xi+1)$ corresponding to

the unidentified coefficients $w_0, \ldots, w_\Xi$, $\Omega_0, \ldots, \Omega_\Xi$, and $\Lambda_0, \ldots, \Lambda_\Xi$. Hence, the algebraic equations can be reformulated as follows:

$$\begin{pmatrix} \mathbb{D}\theta & -I\phi & M_0 \\ M_0 & \mathbb{D}^2\phi & -I\phi \\ \emptyset_{11} & \emptyset_{12} & \emptyset_{13} \end{pmatrix} X = c \begin{pmatrix} M_0 & M_0 & M_0 \\ M_0 & M_0 & M_0 \\ (ia^3\,\mathrm{Re} + ia^5\,\mathrm{Re}\,\eta)I\theta & -(ia\,\mathrm{Re} + 2ia^3\,\mathrm{Re}\,\eta)\mathbb{D}\phi & ia\,\mathrm{Re}\,\eta\mathbb{D}\phi \end{pmatrix} X, \tag{4.9}$$

where $X = (w_0^f, \ldots, w_\Xi^f, \Omega_0, \ldots, \Omega_\Xi, \Lambda_0, \ldots, \Lambda_\Xi)$, M_0 is the zero matrix,

$$\begin{aligned}
&\emptyset_{11}\theta(\xi_1,\xi_2) = [a^4 + a^6K + ia\,\mathrm{Re}(\overline{U}_B(y_{\xi_1})a^2 + (\overline{U}_B)''(y_{\xi_1}))]I\theta(\xi_1,\xi_2),\\
&\emptyset_{12}\phi(\xi_1,\xi_2) = -[2a^2 + 3a^4K + ia\,\mathrm{Re}\,\overline{U}_B(y_{\xi_1})]\mathbb{D}\phi(\xi_1,\xi_2),\\
&\emptyset_{12}\phi(\xi_1,\xi_2) = [1 + 3a^2K]\mathbb{D}\phi(\xi_1,\xi_2) - K\mathbb{D}^3\phi(\xi_1,\xi_2),\\
&I\theta(\xi_1,\xi_2) = \theta_{\xi_2}(y_{\xi_1}), \quad I\phi(\xi_1,\xi_2) = \phi_{\xi_2}(y_{\xi_1}), \quad \mathbb{D}\theta(\xi_1,\xi_2) = \theta'_{\xi_2}(y_{\xi_1}),\\
&\mathbb{D}\phi(\xi_1,\xi_2) = \phi'_{\xi_2}(y_{\xi_1}), \quad \mathbb{D}^2\theta(\xi_1,\xi_2) = \theta''_{\xi_2}(y_{\xi_1}), \quad \mathbb{D}^3\phi(\xi_1,\xi_2) = \phi'''_{\xi_2}(y_{\xi_1}),\\
&\xi_1 = 0, \ldots, \Xi, \quad \xi_2 = 0, \ldots, \Xi.
\end{aligned}$$

We utilised the QZ algorithm from Matlab routines to compute the eigenvalues c_i of system (4.9). After obtaining the eigenvalues c_i, we used the secant method to determine the real and imaginary components of each eigenvalue, denoted as $c_i = c_r + ic_i$. The critical value of the Reynolds number (Re) for a given a^2 is identified at the point where $c_{1r} = 0$, with c_{1r} being the largest real part of the eigenvalues. Following this, the golden section search method was applied to optimize over a^2 and find the critical Re for linear instability.

5. Stability analysis results

This study primarily aims at exploring how the couple stresses parameter (K) and the Kelvin–Voigt parameter (η) influence the critical Reynolds number (Re), the wave number (a), and the critical wave number (a_c). One of the most important parts of this analysis is finding out how many collocation points are enough to guarantee the accuracy and reliability of the results when using both Method I and Method II in the Chebyshev collocation scheme. Several sets of collocation points, symbolized by Ξ, have been used to calculate the critical Reynolds number (Re_c) for various values of η, where $K = 0.005$ is kept constant. The corresponding results are captured in Tables 1 and 2.

The experiment demonstrated in Tables 1 and 2 clearly shows that the calculated Re_c for various ηs initially has inconsistencies with Ξ but eventually

TABLE 1. Re_c for different values of Ξ and η with $K = 0.005$ and for Method I.

η	$\Xi = 40$	$\Xi = 50$	$\Xi = 60$	$\Xi = 70$	$\Xi = 80$	$\Xi = 90$
0.0002	4713.55215	4713.39280	4713.39208	4713.39208	4713.39208	4713.39208
0.00021	4843.98930	4843.73936	4843.73850	4843.73851	4843.73849	4843.73849
0.00022	4982.60293	4982.23426	4982.23324	4982.23324	4982.23325	4982.23325
0.00023	5130.25413	5129.73050	5129.72930	5129.72929	5129.72930	5129.72930
0.00024	5287.93767	5287.21251	5287.21111	5287.21111	5287.21112	5287.21112
0.00025	5456.81014	5455.82386	5455.82222	5455.82222	5455.82223	5455.82223
0.00026	5638.22581	5636.90252	5636.90062	5636.90061	5636.90061	5636.90061
0.00027	5833.78266	5832.02641	5832.02421	5832.02421	5832.02421	5832.02421
0.00028	6045.38225	6043.07312	6043.07065	6043.07068	6043.07064	6043.07064
0.00029	6275.30845	6272.29892	6272.29619	6272.29614	6272.29620	6272.29620
0.0003	6526.33268	6522.44600	6522.44306	6522.44305	6522.44308	6522.44308
0.00031	6801.85679	6796.88968	6796.88671	6796.88671	6796.88670	6796.88670
0.00032	7106.11057	7099.84637	7099.84367	7099.84374	7099.84363	7099.84363
0.00033	7444.43144	7436.67377	7436.67186	7436.67183	7436.67186	7436.67186
0.00034	7823.67104	7814.31796	7814.31787	7814.31796	7814.31786	7814.31786
0.00035	8252.80806	8242.00389	8242.00741	8242.00751	8242.00733	8242.00733
0.00036	8743.91462	8732.34776	8732.35810	8732.35805	8732.35807	8732.35807
0.00037	9313.77643	9303.24864	9303.27127	9303.27126	9303.27137	9303.27137
0.00038	9986.83873	9981.32922	9981.37405	9981.37419	9981.37424	9981.37424
0.00039	10801.19388	10808.79442	10808.87946	10808.87947	10808.87952	10808.87952
0.0004	11822.57450	11858.79068	11858.94976	11858.94972	11858.94976	11858.94976

becomes more and more stable as the number of collocation points grows, thus showing the convergence of both methods. Having $\Xi = 90$ is of a precision level of at least six significant digits. Method II, on the other hand, is significant for reaching the set accuracy in a more cost-efficient way since it needs less collocation points. Therefore, Method II was used hereafter, and $\Xi = 100$ was selected for all the runs to ensure continuity and dependability.

Method I is a very satisfactory choice for hydrodynamic stability problems due to its accuracy and flexibility. However, it takes more CPU time and more polynomials to reach similar accuracy levels when compared to Method II. On the other hand, Method II is more accurate and uses less polynomials for significant accuracy and faster convergence, even though it is less flexible. This is a very beneficial feature for lengthy hydrodynamic stability investigations.

By employing a smaller number of Chebyshev polynomials, Method II manages to maintain the desired accuracy, thus resulting in simpler eigenvalue matrices. Interestingly, in order to keep remarkable accuracy, Method II primarily relies on even, numbered polynomials, such as $T_0, T_2, \ldots$.

Table 2. Re_c for different values of Ξ and η with $K = 0.005$ and for Method II.

η	$\Xi = 30$	$\Xi = 40$	$\Xi = 50$	$\Xi = 60$
0.0002	4713.39208	4713.39207	4713.39208	4713.39208
0.00021	4843.73850	4843.73850	4843.73849	4843.73849
0.00022	4982.23325	4982.23324	4982.23325	4982.23325
0.00023	5129.72931	5129.72930	5129.72930	5129.72930
0.00024	5287.21111	5287.21111	5287.21112	5287.21112
0.00025	5455.82222	5455.82221	5455.82223	5455.82223
0.00026	5636.90061	5636.90060	5636.90061	5636.90061
0.00027	5832.02423	5832.02422	5832.02421	5832.02421
0.00028	6043.07064	6043.07064	6043.07064	6043.07064
0.00029	6272.29619	6272.29618	6272.29620	6272.29620
0.0003	6522.44305	6522.44306	6522.44308	6522.44308
0.00031	6796.88670	6796.88670	6796.88670	6796.88670
0.00032	7099.84367	7099.84365	7099.84363	7099.84363
0.00033	7436.67188	7436.67185	7436.67186	7436.67186
0.00034	7814.31790	7814.31791	7814.31786	7814.31786
0.00035	8242.00743	8242.00743	8242.00733	8242.00733
0.00036	8732.35812	8732.35815	8732.35807	8732.35807
0.00037	9303.27132	9303.27141	9303.27137	9303.27137
0.00038	9981.37409	9981.37422	9981.37424	9981.37424
0.00039	10808.87955	10808.87996	10808.87952	10808.87952
0.0004	11858.94980	11858.94985	11858.94976	11858.94976

From the Orr–Sommerfeld equation, eigenvalues are generally complex. The imaginary part corresponds to oscillatory behavior while the real part controls the growth or decay of perturbations over time. The distribution of these eigenvalues in the complex plane reveals the general pattern of the spectrum. When the Reynolds number is low enough, the flow is stable because all the eigenvalues have a negative real part. This means that the disturbances in the system will fade away and thus the flow will remain laminar.

As the Reynolds number increases, there is a group of eigenvalues with positive real parts, which indicates that disturbances can grow exponentially, thus the flow can become unstable. The critical Reynolds number, Re_c, is the point when the first eigenvalue with a positive real part appears. These unstable eigenvalues often represent a continuous branch in the complex plane, going from the origin to positive real values. The exact form and direction of this branch depend on the flow configuration and the boundary conditions used. At the same time, the imaginary parts of these eigenvalues are the frequencies of the oscillations of the disturbances that are becoming bigger. Typically, higher

Reynolds numbers correspond to disturbances oscillating at higher frequencies, which means that the instability evolves faster.

A deeper insight into the stability characteristics of the flow can be obtained by examining both the growth rate-given by the positive real part of the most unstable eigenvalue-and the corresponding spatial structures, represented by the eigenfunctions associated with the instability. The behavior of the spectrum, as described by Eqs. (3.13) and (3.14), closely resembles that of the classical Poiseuille flow in the Orr–Sommerfeld problem, which serves as a fundamental benchmark in fluid dynamics.

Figures 1 and 2 illustrate the spectral growth rate $c = c_r + ic_i$ results of Methods I and II, respectively. From the pictures, the skewness of the "tail" of the figures lessens if the number of polynomials is increased. However, if one pursues the elimination of the tail skewness too closely, one will start making

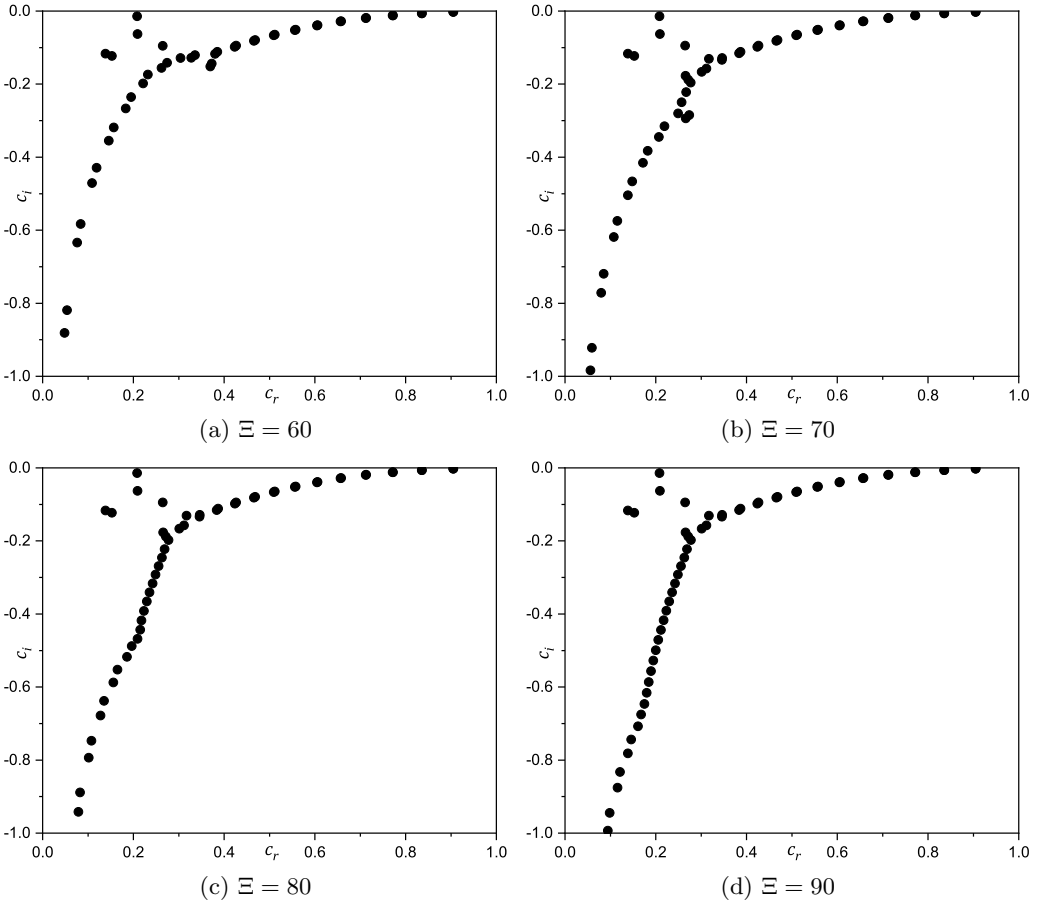

(a) $\Xi = 60$ (b) $\Xi = 70$

(c) $\Xi = 80$ (d) $\Xi = 90$

FIG. 1. Spectral of growth rate $c = c_r + ic_i$ for Method I with $\eta = 0.0004$, $K = 0.005$, $a = 1$ and $\mathrm{Re} = 100000$.

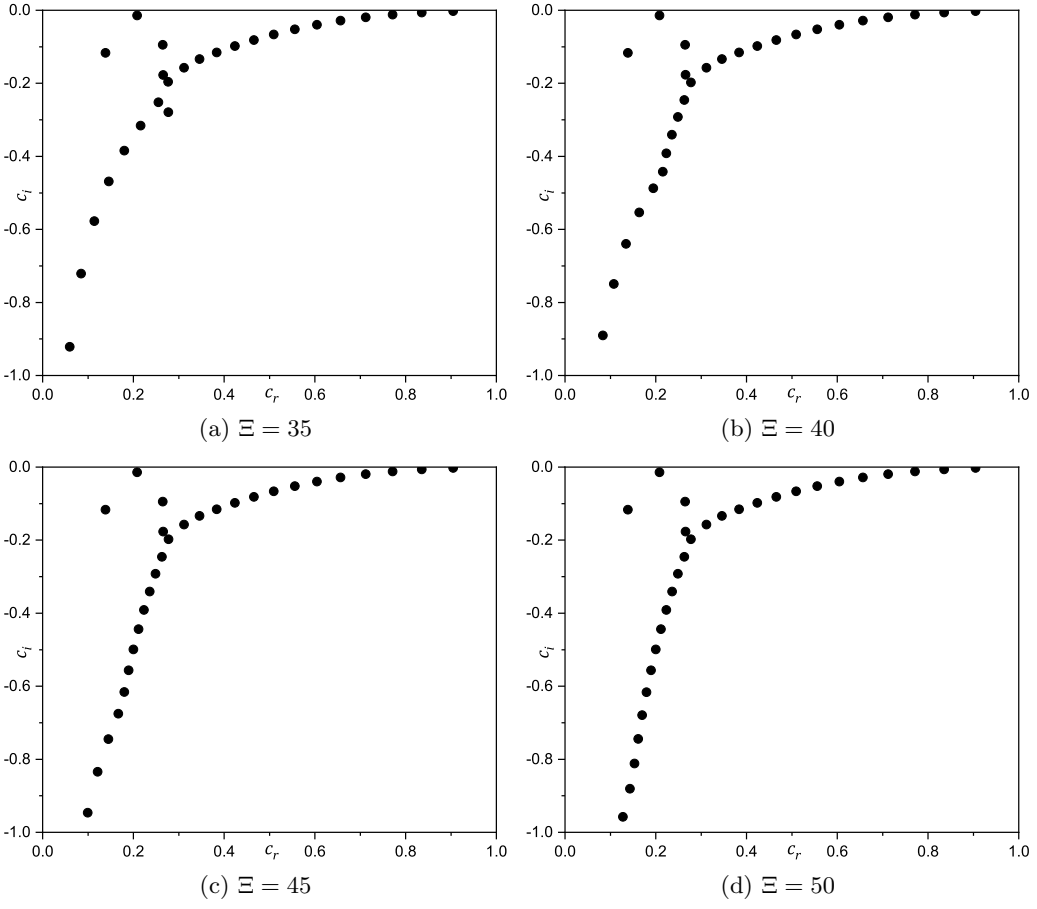

(a) $\Xi = 35$ (b) $\Xi = 40$

(c) $\Xi = 45$ (d) $\Xi = 50$

Fig. 2. Spectral of growth rate $c = c_r + ic_i$ for Method II with $\eta = 0.0004$, $K = 0.005$, $a = 1$ and $\mathrm{Re} = 100000$.

errors at the peak, as it was discovered in [58, 59]. A side by side comparison between Figs. 1 and 2 reveals that Method II manages to reduce the amount of skewness in the tail with fewer polynomials than Method I, which is further evidence of the numerical stability of Method II.

Table 3 compares our study and a previous investigation in [42] with a side by side presentation of some key parameters such as the Reynolds number Re_c, wave number a_c and wave speed c_c. It should be kept in mind that the earlier work did not consider couple stress, so we have taken the case where the couple stress parameter is zero $K = 0$. The table data indicates that the critical Reynolds numbers Re_c from both the studies are in very close agreement, being precise to at least five decimal places. Similarly, the values of a_c and c_c are in agreement, coinciding up to six decimal places.

TABLE 3. Comparison between the critical Reynolds number Re_c, the critical wave number a_c, and the critical wave speed c_c of [42] and this paper for $K = 0$.

η	Present & $K = 0$			[42]		
	Re_c	a_c	c_c	Re_c	a_c	c_c
0	5772.221816	1.020547	0.264000	5772.221817	1.020547	0.264000
10^{-8}	5772.654702	1.020532	0.263994	5772.654703	1.020532	0.263994
10^{-6}	5815.883702	1.019037	0.263463	5815.883703	1.019037	0.263463
10^{-5}	6246.323550	1.004931	0.258440	6246.323551	1.004931	0.258440

Figures 3(a) and (b) depict the effects of changes in the parameter K on the critical Reynolds number, Re_c, at various η levels. On the other hand, Figs. 3(c) and (d) illustrate the Re_c changes with η for different K values. The graphs here

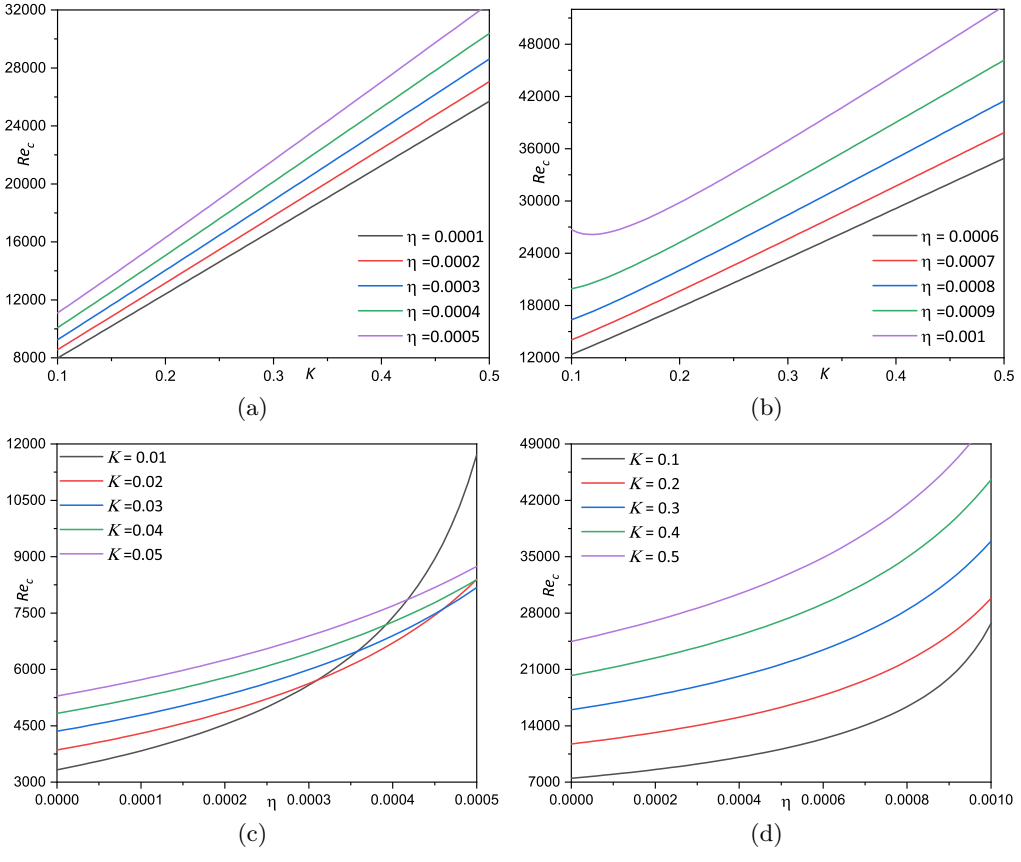

FIG. 3. The critical Reynolds number Re_c against K for different values of η in (a) and (b), and against η for different values of K in (c) and (d).

show stable and unstable zones: the domains under the curves correspond to stability, in which the disturbances tend to decrease, while the domains above the curves correspond to instability, which is characterized by at least one positive eigenvalue being present. The overall drop in Re_c with increases in K and η highlights the effect of these factors on flow instability in these figures. The relationship between (Re_c) and (K) and (η) shows that Re_c begins to rise dramatically at larger levels, particularly as K increases. Stronger couple stresses increase the fluid's resistance to deformation caused by internal micro-rotations. This added resistance can suppress flow perturbations and stabilise the flow against instabilities. Also, at higher levels, the couple stresses effectively increase the system's rotational stiffness and the energy required to create instabilities. This leads to an increase in the critical Reynolds number, meaning that higher flow velocities (or higher Reynolds numbers) are now required to induce instability. Thus, the fluid becomes more stable as the value of the couple stresses increases.

When the Kelvin–Voigt parameter (especially related to viscosity begins to increase, the stabilisation effect becomes more pronounced. This happens because the dominant factor becomes the increased dissipation of energy due to higher viscosity. In simpler terms, the fluid becomes "thicker" and more resistant to fluctuations and disturbances that might otherwise grow under less viscous conditions. Higher viscoelasticity thus dampens instabilities and raises the critical Reynolds number, indicating a stabilisation of the flow. The behaviour at lower and higher values of the Kelvin–Voigt parameter can be seen as a transition from a regime where the flow dynamics are being altered by the introduction of new behaviour (viscoelasticity), which might not initially fit well with the existing flow regime, to a regime where the viscoelastic effects dominate and stabilise the flow through increased dissipation and resistance to deformation.

Figure 4 presents the relationship between the critical wave number a_c and the parameters K and η. The curves displayed illustrate how the critical wave speed c_c varies as a function of K in panels (a) and (b), and as a function of η in panels (c) and (d). As observed in this figure, the critical wave number a_c exhibits distinct responses to changes in these parameters. Figures 4(a) and (b) show that increasing the value of K leads to an increase in the critical wave number. The fluid resists rotational deformation more when the couple stress parameter rises. This indicates that the fluid is less vulnerable to variations in the way its constituent particles rotate. Additionally, this higher resistance keeps the fluid flow stable in the face of disturbances. Put differently, the fluid exhibits enhanced resistance to minor perturbations, hence postponing the start of instabilities. Moreover, the critical wave number rises as a result of the stabilising effect. In terms of physics, this means that in order to disrupt the flow, smaller wavelength disturbances (or greater spatial frequency) are now necessary. The instability threshold thus moves to greater wave numbers.

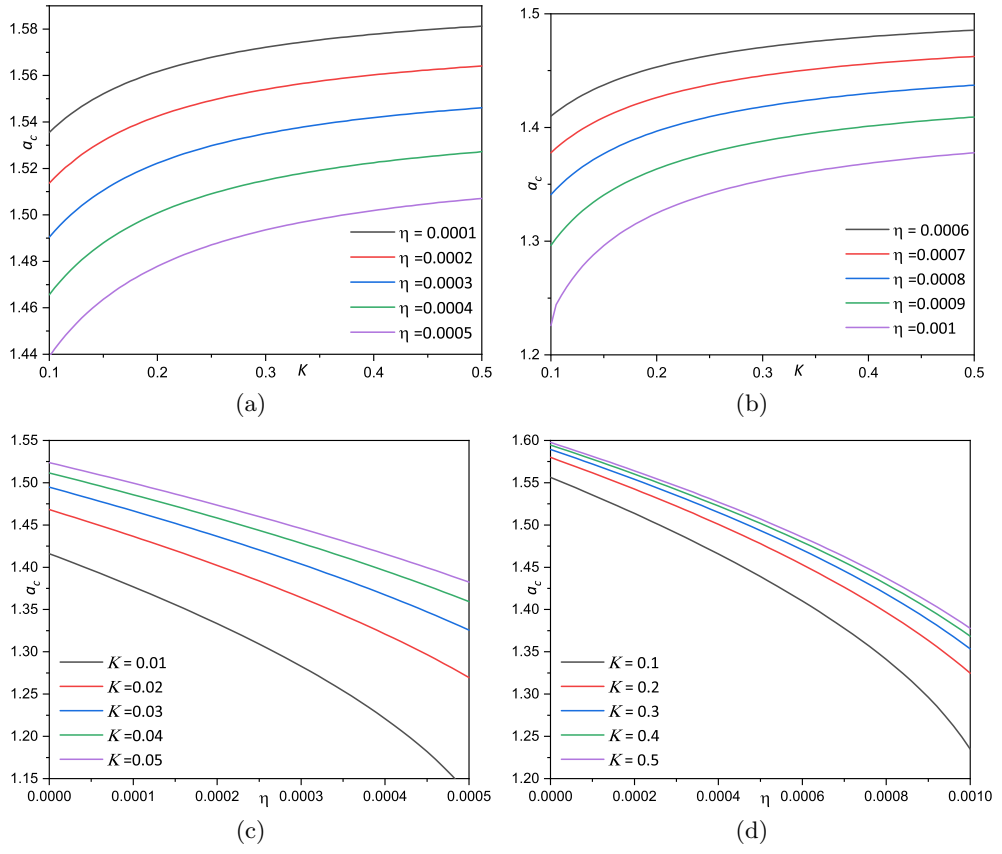

FIG. 4. Critical wave number a_c against K for different values of η in (a) and (b), and against η for different values of K in (c) and (d).

From Figs. 4(c) and (d), we note also that increasing the value of η leads to a decrease in the critical value of the wave number. When the Kelvin–Voigt parameter increases, the following effects occur. First, viscous damping increases with greater values of the Kelvin–Voigt parameter. As a result, the amplitude of disturbances will gradually decrease due to the fluid's increased ability to disperse energy. Additionally, when damping occurs, the fluid's elasticity rises, aiding in the fluid's ability to return to its initial condition following disturbance. This elastic recovery prevents disturbances from growing. Additionally, as a result of the enhanced damping and elasticity, the fluid becomes more stable in response to disturbances of short wavelengths. Consequently, the flow is now more susceptible to destabilisation by disturbances with longer wavelengths (lower spatial frequencies). The critical wave number decreases as a result of this shift, suggesting that instability can be caused by disturbances at lower frequencies.

The critical c_c is examined in Fig. 5 in connection with variations of K and η. Figure 5(a) and (b) illustrate how c_c changes with K for various η values, while Fig. 5(c) and (d) show how c_c varies with η for various K values. Figure 5(a) shows a trend where c_c tends to increase as the parameter K rises. A fluid with a higher couple stresses factor is more resistant to deformations caused by rotation. Additional moments and forces operating inside the fluid to oppose changes in the rotational motion of fluid particles are the cause of this resistance. Furthermore, the fluid's stiffness is effectively increased by the increased rotational resistance. This is due to the fact that the couple stresses give the conventional stresses a rotating component by contributing to the total stress tensor. Furthermore, fluid disturbances can spread more quickly because of the increased stiffness and rotational resistance. This is comparable to the way waves move more quickly through harder media than through softer ones.

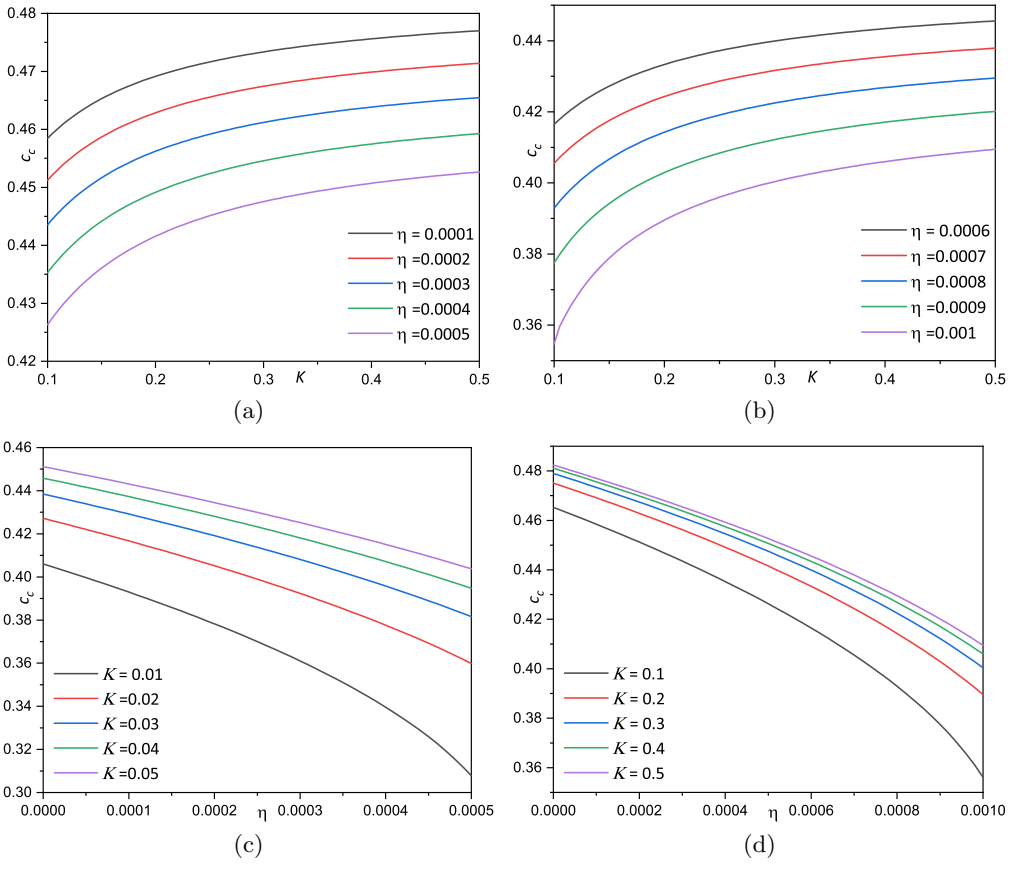

FIG. 5. Critical wave speed c_c against K for different values of η in (a) and (b), and against η for different values of K in (c) and (d).

Because of its improved microstructure's ability to transfer disturbances more effectively, the fluid's greater stiffness enables the fluid to support higher wave speeds.

From Fig. 5(c) and (d), we note that the increase in η results in a significant decrease in the critical wave speed. The Kelvin–Voigt parameter represents the viscous component of the fluid. Higher viscous resistance to deformation corresponds with higher values of η. The wave amplitude is attenuated as a result of this enhanced damping effect's tendency to disperse energy from the propagating waves. Furthermore, the energy available for wave propagation is decreased due to the increased viscous damping. As a result of the viscous forces acting to oppose the motion of the wavefront and hence slow down the transmission of disturbances, waves move through the fluid more slowly. Additionally, the critical wave speed drops as a result of the increased damping. This implies that a wave can move at a lower minimum speed before it is totally damped out. In a viscoelastic medium with a greater Kelvin–Voigt value, waves must propagate more slowly to keep their energy dissipation due to the increased viscosity.

6. Conclusions

Our research focuses on developing computational methods to identify instability thresholds in simulations of complex fluids, similar to those described by the Kelvin–Voigt model, while considering the effects of couple stress. To ensure reliable results, we leverage Squire's theorem, which suggests inherently greater stability in two-dimensional (2D) fluid motion compared to three-dimensional (3D) flow. This allows us to concentrate on 2D stability analysis.

To solve the problem of eigenvalues resulting from linear analysis, two Chebyshev collocation methods were adopted. These methods are considered appropriate ways to deal with this type of problem, especially with regard to boundary conditions. Furthermore, these methods are highly efficient in approximating derivatives numerically. Therefore, these methods are necessary to study the instability of fluid flow in the current model and similar models. These methods were used to determine critical thresholds for linear instability with very high efficiency and accuracy.

There are some conclusions drawn from the current study, which can be summarized as follows:

1. For fluid flow issues, increasing the couple stress factor increases stability through a number of ways involving changes to the fluid's viscosity, microstructural behaviour, and interaction with external forces.
2. The couple stress factor introduces additional stress terms because the fluid's particles can resist deformation and help stabilize the flow. This mechanism

is highlighted in [60], who investigated couple-stress fluid helical flows inside a circular cylinder.

3. Improved stability is a result of the couple stress parameter's reduction in drag force, pressure, and fluid velocity. The work in [61] on the creeping flow of couple stress fluid past a fluid sphere provides evidence of this stabilising impact.
4. When compared to typical viscous fluids, the couple stress parameter increases drag by providing resistance to flow. According to a research on oscillating flow across a permeable sphere in [62], this additional resistance stabilises the flow.
5. For fluid flow issues, increasing the Kelvin–Voigt factor increases stability through a number of methods including viscosity changes, shear effects, and energy dissipation.
6. The viscosity of a fluid is represented by the Kelvin–Voigt factor. Higher viscosity, which improves kinetic energy dissipation and attenuates flow disturbances, is indicated by higher values of this characteristic. This is especially clear from the work in [63], whereby Kelvin–Helmholtz instability is stabilised by raising the Kelvin–Voigt factor through altering the relative velocity's critical value.
7. By increasing the Kelvin–Voigt factor, the shear term's contribution to the generation of disturbance kinetic energy – which stabilises the flow – is increased. In [64], this mechanism is studied in the context of convection-diffusion of binary mixtures.

Data availability

The data that supports the findings of this study are available within the article.

Conflict of interest

We have no competing interests.

Acknowledgments

We would like to express our gratitude to two anonymous referees for their valuable feedback and insightful comments, which have greatly contributed to the enhancement of this manuscript.

References

1. P.G. DRAZIN, W.H. REID, *Hydrodynamic Stability*, 2nd ed., Cambridge University Press, Cambridge, 2004, https://doi.org/10.1017/CBO9780511616938.
2. W.M'F. ORR, *The stability or instability of the steady motions of a perfect liquid and of a viscous liquid. Part II: A viscous liquid*, Proceedings of the Royal Irish Academy. Section A: Mathematical and Physical Sciences, **27**, 69–138, 1907.
3. A. SOMMERFELD, *Ein Beitrag zur hydrodynamischen Erklärung der turbulenten Flüssigkeitsbewegung*, Proceedings of the 4th International Mathematical Congress, **3**, 116–124, 1908/1909.
4. R.C. LOCK, *The stability of the flow of an electrically conducting fluid between parallel planes under a transverse magnetic field*, Proceedings of the Royal Society of London. Series A. Mathematical and Physical Sciences, **233**, 1192, 105–125, 1955, https://doi.org/10.1098/rspa.1955.0249.
5. T. KAKUTANI, *The hydromagnetic stability of the modified plane Couette flow in the presence of a transverse magnetic field*, Journal of the Physical Society of Japan, **19**, 6, 1041–1057, 1964, https://doi.org/10.1143/JPSJ.19.1041.
6. B.M. SHANKAR, I.S. SHIVAKUMARA, *Benchmark solution for the stability of plane Couette flow with net throughflow*, Scientific Reports, **11**, 10901, 2021, https://doi.org/10.1143/JPSJ.19.1041.
7. D.A. NIELD, *The stability of flow in a channel or duct occupied by a porous medium*, International Journal of Heat and Mass Transfer, **46**, 22, 4351–4354, 2003, https://doi.org/10.1016/S0017-9310(03)00105-4.
8. B.M. SHANKAR, I.S. SHIVAKUMARA, J. KUMAR, *Benchmark solution for the hydrodynamic stability of plane porous-Couette flow*, Physics of Fluids, **32**, 10, 104104, 2020, https://doi.org/10.1063/5.0014093.
9. Z.A. AFLUK, A.J. HARFASH, *Instability of thermosolutal convection in a Brinkman–Darcy–Kelvin–Voigt fluid*, Journal of Porous Media, **28**, 2, 1–19, 2025, https://doi.org/10.1615/JPorMedia.2024050970.
10. A.J. BADDAY, A.J. HARFASH, *Thermal convection in rotating bi-disperse porous medium with local thermal nonequilibrium*, Heat Transfer, **54**, 6, 3723–3737, 2025, https://doi.org/10.1002/htj.23380.
11. S.L. KHALAF, A.J. HARFASH, *Hydrodynamic stability of convection in porous medium with chemical reaction effect and generalised boundary conditions*, Physica D: Nonlinear Phenomena, **483**, 135007, 2025, https://doi.org/10.1016/j.physd.2025.135007.
12. S.L. KHALAF, A.J. HARFASH, *Convection in porous medium using Darcy–Brinkman model with chemical reaction and higher concentration gradient effects*, Physics of Fluids, **37**, 10, 104122, 2025, https://doi.org/10.1063/5.0289816.
13. S.L. KHALAF, A.J. HARFASH, *Thermosolutal convection in dual-porosity media with generalized boundary conditions and magnetic field effect*, Heat Transfer, **54**, 7, 4351–4371, 2025, https://doi.org/10.1002/htj.23415.
14. S.S. HAJOOL, A.J. HARFASH, *Instability in Poiseuille flow in a bidisperse porous medium with relatively large macropores*, Special Topics & Reviews in Porous Media: An International Journal, **15**, 3, 27–42, 2024, https://doi.org/10.1615/SpecialTopicsRevPorousMedia.2023048200.

15. S.S. Hajool, A.J. Harfash, *Instability of Poiseuille flow in a bidisperse porous medium subject to a uniform vertical throughflow effect*, Journal of Fluids Engineering, **146**, 5, 051301, 2024, https://doi.org/10.1115/1.4064102.

16. S.S. Hajool, A.J. Harfash, *Hydrodynamic stability of Poiseuille flow in a bidisperse porous medium with slip effect*, International Journal of Modern Physics B, **39**, 1, 2550006, 2025, https://doi.org/10.1142/S0217979225500067.

17. S. Debnath, A.K. Roy, O.A. Bég, *Reactive solute transport in blood flow through a permeable capillary*, Archives of Mechanics, **74**, 2–3, 173–200, 2022, https://doi.org/10.24423/aom.3955.

18. T. Chattopadhyay, S. Kundu, *Analysis of time-averaged secondary flow cells in wide and narrow straight open channels with lateral bed deformation*, Archives of Mechanics, **75**, 1–2, 169–211, 2023, https://doi.org/10.24423/aom.4139.

19. F. Mendil, S. Mamache, F.N. Bouda, *Stability analysis of MHD stagnation flow over a permeable heated rotating disk with heat generation/absorption*, Archives of Mechanics, **76**, 5, 471–494, 2024, https://doi.org/10.24423/aom.4535.

20. P.K. Meduri, P.N.L. Devi, *Stokes flow over a contaminated fluid sphere embedded in a porous medium with slip condition*, Archives of Mechanics, **76**, 3, 253–275, 2024, https://doi.org/10.24423/aom.4392.

21. M. Turkyilmazoglu, *Bödewadt flow and heat transfer of dusty fluid with Navier slip*, Archives of Mechanics, **74**, 2–3, 157–172, 2022, https://doi.org/10.24423/aom.3930.

22. M.E. Erdogan, *Dynamics of polar fluids*, Acta Mechanica, **15**, 3, 233–253, 1972, https://doi.org/10.1007/BF01304293.

23. V.K. Stokes, *Theories of Fluids with Microstructure: An Introduction*, Springer, Berlin, Heidelberg, 1984, https://doi.org/10.1007/978-3-642-82351-0.

24. T. Ariman, M.A. Turk, N.D. Sylvester, *Microcontinuum fluid mechanics – A review*, International Journal of Engineering Science, **11**, 8, 905–930, 1973, https://doi.org/10.1016/0020-7225(73)90038-4.

25. G.K. Batchelor, *An Introduction to Fluid Dynamics*, Cambridge University Press, Cambridge, 1967, https://doi.org/10.1017/CBO9780511800955.

26. Z.A. Afluk, A.J. Harfash, *Thermal convection in a Brinkman–Darcy and Kelvin–Voigt fluid of order one with coupled stresses effect*, Heat Transfer, **54**, 1, 184–202, 2025, https://doi.org/10.1002/htj.23165.

27. Z.A. Afluk, A.J. Harfash, *Double diffusive convection in bidispersive porous media with couple stresses effect and relatively large macropores*, Numerical Heat Transfer, Part A: Applications, **86**, 10, 3188–3210, 2025, https://doi.org/10.1080/10407782.2023.2299292.

28. Z.A. Afluk, A.J. Harfash, *Stability and instability of thermosolutal convection in a Brinkman–Darcy–Kelvin–Voigt fluid with couple stress effect*, Physics of Fluids, **36**, 3, 034108, 2024, https://doi.org/10.1063/5.0196321.

29. F. Franchi, B. Lazzari, R. Nibbi, *The J–S model versus a non-ideal MHD theory*, Physics Letters A, **379**, 22–23, 1431–1436, 2015, https://doi.org/10.1016/j.physleta.2015.03.026.

30. V. ANAND, J. DAVID JR., I.C. CHRISTOV, *Non-Newtonian fluid–structure interactions: Static response of a microchannel due to internal flow of a power-law fluid*, Journal of Non-Newtonian Fluid Mechanics, **264**, 62–72, 2019, https://doi.org/10.1016/j.jnnfm.2018.12.008.

31. S. CHIRIŢĂ, V. ZAMPOLI, *On the forward and backward in time problems in the Kelvin–Voigt thermoviscoelastic materials*, Mechanics Research Communications, **68**, 25–30, 2015, https://doi.org/10.1016/j.mechrescom.2015.03.007.

32. X.-G. YANG, L. LI, Y. LU, *Regularity of uniform attractor for 3D non-autonomous Navier–Stokes–Voigt equation*, Applied Mathematics and Computation, **334**, 11–29, 2018, https://doi.org/10.1016/j.amc.2018.03.096.

33. O.P. MATVEEVA, *Model of thermoconvection of incompressible viscoelastic fluid of nonzero order. Computational experiment*, Vestnik Yuzhno-Ural'skogo Universiteta, Seriya Matematicheskoe Modelirovanie i Programmirovanie, **6**, 1, 134–138, 2013.

34. B. STRAUGHAN, *Stability for the Kelvin–Voigt variable order equations backward in time*, Mathematical Methods in the Applied Sciences, **44**, 17, 12537–12544, 2021, https://doi.org/10.1002/mma.7559.

35. B. STRAUGHAN, *Thermosolutal convection with a Navier–Stokes–Voigt fluid*, Applied Mathematics and Optimization, **84**, 3, 2587–2599, 2021, https://doi.org/10.1007/s00245-020-09719-7.

36. B. STRAUGHAN, *Continuous dependence and convergence for a Kelvin–Voigt fluid of order one*, Annali dell'Università di Ferrara, **68**, 49–61, 2022, https://doi.org/10.1007/s11565-021-00381-7.

37. B. STRAUGHAN, *Nonlinear stability for convection with temperature dependent viscosity in a Navier–Stokes–Voigt fluid*, The European Physical Journal Plus, **138**, 5, 438, 2023, https://doi.org/10.1140/epjp/s13360-023-04055-5.

38. B. STRAUGHAN, *Effect of temperature upon double diffusive instability in Navier–Stokes–Voigt models with Kazhikhov–Smagulov and Korteweg terms*, Applied Mathematics and Optimization, **87**, 3, 54, 2023, https://doi.org/10.1007/s00245-023-09964-6.

39. A.J. BADDAY, A.J. HARFASH, *The effects of the Soret and slip boundary conditions on thermosolutal convection with a Navier–Stokes–Voigt fluid*, Physics of Fluids, **35**, 1, 014101, 2023, https://doi.org/10.1063/5.0128993.

40. A.J. BADDAY, A.J. HARFASH, *Thermosolutal convection in a Brinkman–Darcy–Kelvin–Voigt fluid with a bidisperse porous medium*, Physics of Fluids, **36**, 1, 014119, 2024, https://doi.org/10.1063/5.0186934.

41. R.G. LARSON, *Instabilities in viscoelastic flows*, Rheologica Acta, **31**, 3, 213–263, 1992, https://doi.org/10.1007/BF00366504.

42. B.M. SHANKAR, I.S. SHIVAKUMARA, *Stability of plane Poiseuille and Couette flows of Navier–Stokes–Voigt fluid*, Acta Mechanica, **234**, 10, 4589–4609, 2023, https://doi.org/10.1007/s00707-023-03624-0.

43. G.N. KAVITHA, B.M. SHANKAR, I.S. SHIVAKUMARA, *On the magnetohydrodynamic stability of channel flow of Navier–Stokes–Voigt fluid*, Physics of Fluids, **36**, 4, 043105, 2024, https://doi.org/10.1063/5.0196788.

44. J. BEAR, *Dynamics of Fluids in Porous Media*, Dover Publications, Mineola, NY, 2013.

45. R.B. Bird, W.E. Stewart, E.N. Lightfoot, *Transport Phenomena*, 2nd ed., John Wiley & Sons, New York, 2006.

46. M. Takashima, *The stability of the modified plane Poiseuille flow in the presence of a transverse magnetic field*, Fluid Dynamics Research, **17**, 6, 293–310, 1996, https://doi.org/10.1016/0169-5983(95)00038-0.

47. M. Takashima, *The stability of the modified plane Couette flow in the presence of a transverse magnetic field*, Fluid Dynamics Research, **22**, 2, 105–121, 1998, https://doi.org/10.1016/S0169-5983(97)00029-4.

48. B.S. Ng, W.H. Reid, *A numerical method for linear two-point boundary-value problems using compound matrices*, Journal of Computational Physics, **33**, 1, 70–85, 1979, https://doi.org/10.1016/0021-9991(79)90028-7.

49. B.S. Ng, W.H. Reid, *The compound matrix method for ordinary differential systems*, Journal of Computational Physics, **58**, 2, 209–228, 1985, https://doi.org/10.1016/0021-9991(85)90177-9.

50. S.G. Yiantsios, B.G. Higgins, *Numerical solution of eigenvalue problems using the compound matrix method*, Journal of Computational Physics, **74**, 1, 25–40, 1988, https://doi.org/10.1016/0021-9991(88)90066-6.

51. S.A. Orszag, *Accurate solution of the Orr–Sommerfeld stability equation*, Journal of Fluid Mechanics, **50**, 4, 689–703, 1971, https://doi.org/10.1017/S0022112071002842.

52. S.S. Hajool, A.J. Harfash, *Magnetohydrodynamic instability of fluid flow in a bidisperse porous medium*, Journal of Engineering Mathematics, **147**, 10, 2024, https://doi.org/10.1007/s10665-024-10369-9.

53. S.S. Hajool, A.J. Harfash, *Instability of Poiseuille flow of viscoelastic fluids in a porous medium of Brinkman–Darcy–Kelvin–Voigt type with slip effect*, Journal of Applied and Computational Mechanics, **11**, 3, 797–810, 2025, https://doi.org/10.22055/jacm.2024.47962.4876.

54. S.S. Hajool, A.J. Harfash, *Instability of Poiseuille flow in a porous medium with couple stresses effect*, Journal of Porous Media, **28**, 8, 109–125, 2025, https://doi.org/10.1615/JPorMedia.2024054524.

55. W.K. Ghafil, A.J. Harfash, H.A. Challoob, A.J. Harfash, *Instability of thermal convection in a porous layer saturated with a nanofluid using general boundary conditions*, International Journal of Numerical Methods for Heat & Fluid Flow, **36**, 2, 1043–1075, 2026, https://doi.org/10.1108/HFF-09-2025-0729.

56. S.L. Khalaf, A.J. Harfash, *Double-diffusive convection in a Darcy–Brinkman porous layer with higher-order thermal and solutal diffusion*, International Journal of Numerical Methods for Heat & Fluid Flow, **36**, 5, 1993–2026, 2026, https://doi.org/10.1108/HFF-12-2025-1000.

57. S.L. Khalaf, A.J. Harfash, *Instability and stability analysis of double-diffusive convection in Kelvin–Voigt fluids with internal heating*, International Communications in Heat and Mass Transfer, **175**, Part 2, 111123, 2026, https://doi.org/10.1016/j.icheatmasstransfer.2026.111123.

58. J.J. Dongarra, B. Straughan, D.W. Walker, *Chebyshev tau–QZ algorithm methods for calculating spectra of hydrodynamic stability problems*, Applied Numerical Mathematics, **22**, 4, 399–434, 1996, https://doi.org/10.1016/S0168-9274(96)00049-9.

59. P. YECKO, *Disturbance growth in two-fluid channel flow: The role of capillarity*, International Journal of Multiphase Flow, **34**, 3, 272–282, 2008, https://doi.org/10.1016/j.ijmultiphaseflow.2007.09.005.

60. Q. RUBBAB, I.A. MIRZA, I. SIDDIQUE, S. IRSHAD, *Unsteady helical flows of a size-dependent couple-stress fluid*, Advances in Mathematical Physics, **2017**, 9724381, 2017, https://doi.org/10.1155/2017/9724381.

61. R. KRISHNAN, P. SHUKLA, *Creeping flow of couple stress fluid past a fluid sphere with a solid core*, ZAMM – Journal of Applied Mathematics and Mechanics/Zeitschrift für Angewandte Mathematik und Mechanik, **101**, 11, e202000115, 2021, https://doi.org/10.1002/zamm.202000115.

62. P. APARNA, P. PADMAJA, N. POTHANNA, J.V.R. MURTHY, *Couple stress fluid flow due to slow steady oscillations of a permeable sphere*, Nonlinear Engineering, **9**, 1, 352–360, 2020, https://doi.org/10.1515/nleng-2020-0021.

63. T. FUNADA, D.D. JOSEPH, *Viscous potential flow analysis of Kelvin–Helmholtz instability in a channel*, Journal of Fluid Mechanics, **445**, 263–283, 2001, https://doi.org/10.1017/S0022112001005572.

64. M.K. KHANDELWAL, N. SINGH, A.K. SHARMA, P. YU, *Instabilities during convection–diffusion of binary mixtures in a non-isothermal flow: A linear stability analysis*, Physics of Fluids, **33**, 8, 084107, 2021, https://doi.org/10.1063/5.0059313.

Received February 12, 2026; revised version May 28, 2026.
Published online 11 June, 2026.